in vivo *37*: 132-142 (2023)
doi:10.21873/invivo.13062

Age-related Changes in Trigeminal Ganglion Macrophages Enhance Orofacial Ectopic Pain After Inferior Alveolar Nerve Injury

SHINTARO FUJIWARA[1], KENTARO URATA[1], TATSUKI OTO[1], YOSHINORI HAYASHI[2], SUZURO HITOMI[2], KOICHI IWATA[2], TOSHIMITSU IINUMA[1] and MASAMICHI SHINODA[2]

[1]*Department of Complete Denture Prosthodontics, Nihon University School of Dentistry, Tokyo, Japan;*
[2]*Department of Physiology, Nihon University School of Dentistry, Tokyo, Japan*

Abstract. *Background/Aim: The ectopic pain associated with inferior alveolar nerve (IAN) injury has been reported to involve macrophage expression in the trigeminal ganglion (TG). However, the effect of age-related changes on this abnormal pain conditions are still unknown. This study sought to clarify the involvement of age-related changes in macrophage expression and phenotypic conversion in the TG and how these changes enhance ectopic mechanical allodynia after IAN transection (IANX). Materials and Methods: We used senescence-accelerated mouse (SAM)-prone 8 (SAMP8) and SAM-resistance 1 (SAMR1) mice, which are commonly used to study ageing-related changes. Mechanical stimulation was applied to the whisker pad skin under light anaesthesia; the mechanical head withdrawal threshold (MHWT) was measured for 21 d post-IANX. We subsequently counted the numbers of Iba1 (macrophage marker)-immunoreactive (IR) cells, Iba1/CD11c (M1-like inflammatory macrophage marker)-co-IR cells, and Iba1/CD206 (M2-like anti-inflammatory macrophage marker)-co-IR cells in the TG innervating the whisker pad skin. After continuous intra-TG administration of liposomal clodronate Clophosome®-A (LCCA) to IANX-treated SAMP8-mice, the MHWT values of the whisker pad skin were examined. Results: Five days post-IANX, the MHWT had significantly decreased in SAMP8 mice compared to SAMR1-mice. Iba1-IR and Iba1/CD11c-co-IR cell counts were significantly increased in SAMP8 mice compared to SAMR1 mice 5 d post-IANX. LCCA administration significantly restored MHWT compared to control-LCCA administration. Conclusion: Ectopic mechanical allodynia of whisker pad skin after IANX is exacerbated by ageing, which involves increases in M1-like inflammatory macrophages in the TG.*

Correspondence to: Kentaro Urata, DDS, Ph.D., Department of Complete Denture Prosthodontics, Nihon University School of Dentistry, 1-8-13 Kandasurugadai, Chiyoda-ku, Tokyo 101-8310, Japan. Tel: +81 332198143, Fax: +81 332198323, e-mail: urata.kenntarou@nihon-u.ac.jp

Key Words: Macrophage, SAMP8, SAMR1, M1, M2, IANX, orofacial ectopic pain, ageing.

This article is an open access article distributed under the terms and conditions of the Creative Commons Attribution (CC BY-NC-ND) 4.0 international license (https://creativecommons.org/licenses/by-nc-nd/4.0).

Orofacial neuropathic pain usually occurs following trigeminal nerve injury. In clinical settings, injury to the inferior alveolar nerve (IAN) – the third branch of the trigeminal nerve – often caused by implant misplacement, accidents during wisdom tooth extraction, and other invasive dental treatments (1, 2). Recent studies have reported that IAN injury causes not only dysesthesia of lower lip but also abnormal pain in the intact orofacial area outside the IAN-innervated area (3, 4). It is vital for dentists to accurately diagnose and relieve pain, which is crucial to the treatment of patients suffering from abnormal pain.

Primary neuronal hyperexcitability caused by peripheral nerve injury and inflammation induces the release of signalling molecules from primary sensory neuronal soma as well as non-neuronal cells, such as macrophages in the TG (5, 6). Peripheral nerve injury also causes persistent changes in undamaged nerves adjacent to the injured nerve (7). These changes involve not only neuron-neuron communication, but also neuron-glia and neuron-macrophage communication (8-10). Orofacial ectopic pain is also reportedly caused by enhanced excitability of nociceptive TG neurons, and this neuronal hyperexcitability is caused by the activation of satellite glial cells *via* $P2Y_{12}$ receptor signalling, or the enhanced signalling of tumour necrosis factor (TNF)-α release from proliferating and activated macrophages in the TG (11, 12). Macrophages accumulated by nerve injury or inflammation differentiate into two phenotypes with distinct morphological and functional profiles corresponding to the

microenvironment to which they migrate (13). M1-like inflammatory macrophages can secrete numerous inflammatory cytokines and chemokines, thereby affecting local inflammatory responses (14). In contrast, M2-like anti-inflammatory macrophages facilitate anti-inflammatory responses and tissue repair (15). Polarization of these two opposing phenotypes can augment or attenuate pain sensitivity (16, 17); this polarization is also probably involved in the pathogenesis of orofacial ectopic pain.

Neuropathic pain is reportedly exacerbated in the elderly (18, 19). The correlation between ageing and neuropathic pain is reportedly due to age-related changes in macrophage expression in the dorsal root ganglion, which enhances neuropathic pain after sciatic nerve injury (20). Moreover, age-related increases in microglia in the trigeminal spinal subnucleus caudalis enhance the mechanical allodynia of the oral mucosa (21). Thus, changes in immune cell expression in nociceptive signalling pathways are associated with ageing-modulated pain hypersensitivity; however, the role of immune cells of the TG in the orofacial ectopic pain after IAN injury in elderly compared to younger remains unclear.

Recent studies have used senescence-accelerated mice-prone-8 (SAMP8) and SAM-resistant/1 (SAMR1) mice to investigate age-related pathological changes (22-24). SAMP8 mice exhibit learning and memory deficits and show a rapid age-dependent increase in senescence, while SAMR1 mice are the normal ageing control strain for SAMP8 mice (23, 25, 26).

This study aimed to examine age-related changes in macrophage expression and polarity in the TG after IANX and its involvement in the orofacial ectopic mechanical allodynia using SAMP8 and SAMR1 mice.

Materials and Methods

Animals. We used 23-week-old male SAMP8 (n=98, Japan SLC, Shizuoka, Japan), and 23-week-old male SAMR1 (n=56, Japan SLC) mice weighing 20-30 g. All mice were individually housed in clear polycarbonate cages and maintained in a controlled temperature (23˚C) environment under a 12-h light/dark cycle with free access to food and water. All experiments were conducted in accordance with the guidelines of the International Association for the Study of Pain (27) and approved by the Animal Experimentation Committee at Nihon University School of Dentistry (AP19DEN012). The number of mice used in the experiment was the minimum required for statistical analysis.

The inferior alveolar nerve transection model. Inferior alveolar nerve transection (IANX) was performed under deep anaesthesia with intraperitoneal (*i.p.*) administration of butorphanol (5 mg/kg; Meiji Seika, Tokyo, Japan), medetomidine (0.75 mg/kg; Zenoac, Fukushima, Japan), and midazolam (4.0 mg/kg; Sandoz, Tokyo, Japan) as previously described (28, 29). Briefly, a small incision was made in the skin of the left cheek and the masseter muscle was incised. The masseter muscle was dissected to expose the surface of the mandible.

The mandibular surface was scraped with a low-speed dental drill bar to expose the IAN. The exposed IAN was replaced with a mandibular canal after the IAN was gently withdrawn and cut. In the control group, a sham operation was performed, which consisted of skin incision, muscle debridement, and bone shaving without severing the IAN, before the incised muscle and skin incision were sutured with 6-0 silk.

Measuring mechanical sensitivity of the whisker pad skin and lower lip. Mechanical stimulation was conducted after confirming that the mice were maintained at the depth of anaesthesia as described below. Briefly, mice were anaesthetized with 2% isoflurane (Mylan, Canonsburg, PA, USA). After discontinuing the supply of 2% isoflurane, we confirmed whether an identical hind limb withdrawal reflex was induced by identical noxious pinch stimulation to the hind paw and assessing whether the breathing and cardiac rhythm were appropriate. Mice were mechanically stimulated with their heads fixed with silicone rubber to prevent head movement; further, mechanical stimulation was applied to the left whisker pad skin using an electronic von Frey anaesthesiometer (Bioseb, Chaville, France) while they were under constant, adjusted-depth anaesthesia. Mechanical stimulation was also applied to the left lower lip ipsilateral to the IANX conducted site using flat-tipped forceps (Panlab s.l., Barcelona, Spain) while under constant, adjusted-depth anaesthesia. Both mechanical stimulation intensities were gradually increased at a specified rate (von Frey anesthesiometer; 0-100 g, 10 g/s, cut-off: 100 g, flat tipped forceps; 0-80 g, 10 g/s, cut-off: 80 g). The lowest intensity of mechanical stimulation required to induce the head withdrawal reflex was defined as the mechanical head withdrawal reflex threshold (MHWT). Each stimulation interval was 3 min; the average of three measurements was defined as the MHWT for each mouse. MHWT measurements were performed under blinded conditions.

Intra-TG administration of Clophosome®-A. SAMP8 mice were anaesthetized with an *i.p.* injection of butorphanol (5 mg/kg), midazolam (4.0 mg/kg), and medetomidine (0.75 mg/kg). The skull was exposed, and a small hole (1 mm in diameter) was drilled above the TG (2.8 mm anterior from the posterior fontanelle, 1.2 mm lateral to the sagittal suture) ipsilateral to the location of IANX. Next, the guide cannula was extended to the TG (6 mm below the skull surface) through the small hole and then secured to the skull using dental cement. The correct position of the tip of the cannula was confirmed by inserting the trocar as an electrode into the cannula and testing the induction of multi-unit activity by mechanical stimulation of the left whisker pad skin (29). After cannula fixation, a 26-gauge needle, polyethylene tubing (0.8 mm in diameter; Natsume, Tokyo, Japan), and an osmotic mini-pump (0.11 μl/h, Alzet model 1004; Durect Corporation, Cupertino, CA, USA) were connected, and inserted into the TG through the cannula. Subsequently, liposomal clodronate Clophosome®-A (LCCA, 13.2 μl; F70101-CA, FormuMax Scientific, Sunnyvale, CA, USA), plain control liposomes for LCCA (Cont-LCCA, 13.2 μl, F70101-A, FormuMax Scientific), or vehicle were continually administered into the TG before operation and on days 1-5 following IANX or sham operation. Next, under light anaesthesia with 2% isoflurane, the MHWT of the left whisker pad skin and left lower lip were measured before the IANX operation and every other day for 5 d after IANX or sham operation.

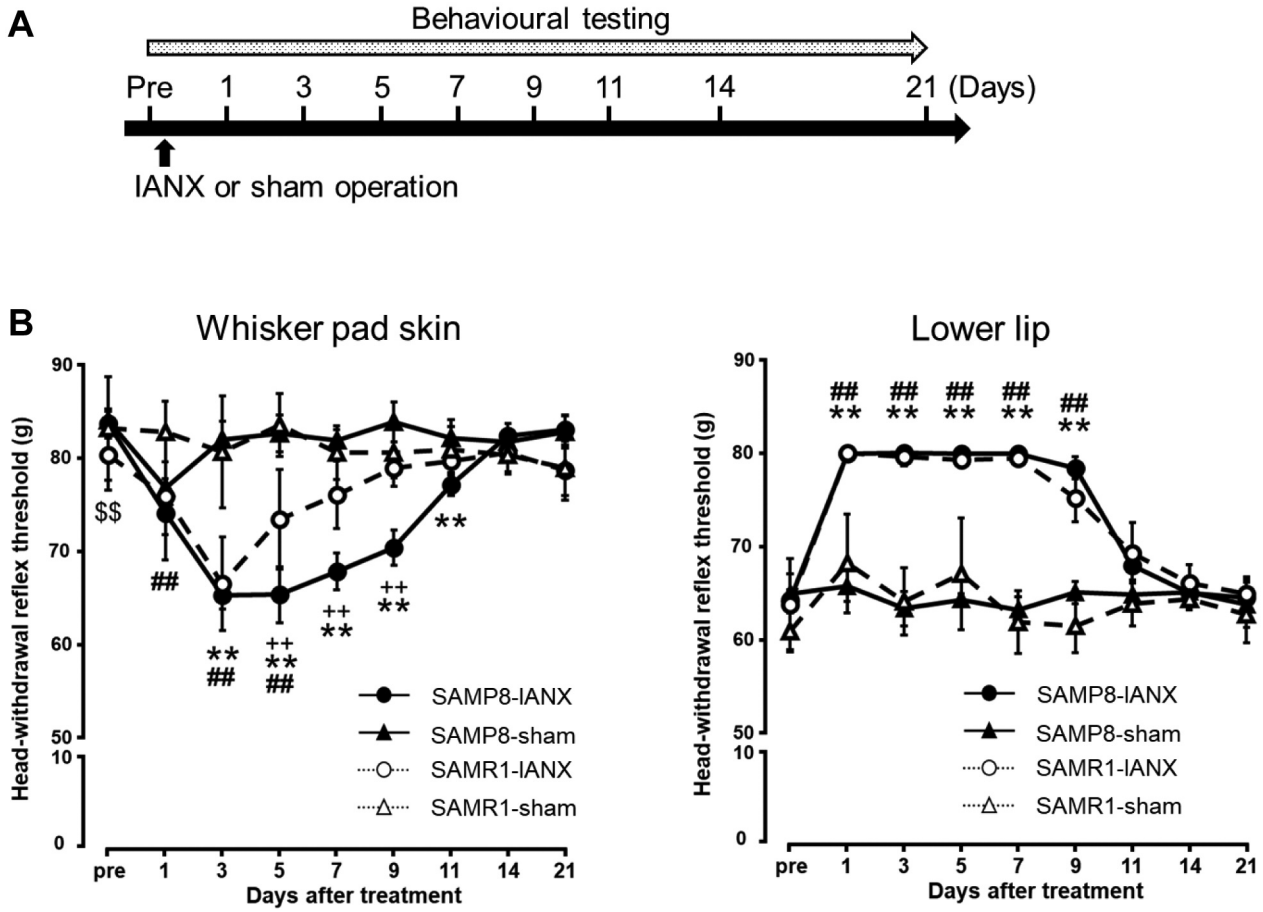

Figure 1. *Changes in mechanical sensitivity of the whisker pad skin and the lower lip following inferior alveolar nerve transection (IANX). (A) Time course of treatment and behavioural testing. (B) Changes in mechanical head withdrawal threshold (MHWT) of the whisker pad skin for 21 d following IANX. Changes in MHWT of the lower lip for 21 d following IANX. Data represent mean±SD. (n=7 each for IANX-treated SAMP8, IANX-treated SAMR1 sham-operated SAMP8, and sham-operated SAMR1 mice; two-way ANOVA with repeated measures followed by Sidak's multiple-comparison tests, **p<0.01, IANX-treated SAMP8 vs. sham-operated SAMP8 mice. ##p<0.01, IANX-treated SAMR1 vs. sham-operated SAMR1 mice. ++p<0.01, IANX-treated SAMP8 vs. IANX-treated SAMR1 mice. $$p<0.01, sham-operated SAMP8 vs. sham-operated SAMR1 mice).*

Immunohistochemistry in TG. Following deep anaesthesia by *i.p.* injection of butorphanol (5 mg/kg), midazolam (4.0 mg/kg), and medetomidine (0.75 mg/kg), we injected a retrograde labelling tracer, 4% FluoroGold (FG, 5 μl dissolved in saline; Fluorochrome, Denver, CO, USA) into the left whisker pad skin using a 30-gauge needle 7 d before IANX or the sham operation. On day 5 after the IANX operation, the mice were transcardially perfused with saline followed by a mixture of 4% paraformaldehyde (PFA) in 0.1 M phosphate buffer (PB; pH=7.4). After fixation, the ipsilateral TG was dissected out and immersed in the same fixative component at 4˚C for 24 h and then kept in 0.01 M phosphate buffer saline (PBS) containing 20% sucrose for 6 h for cryoprotection. Next, the TGs were embedded in Tissue-Tek® (Sakura Finetek, Tokyo, Japan) and stored at –20˚C until cryosectioning.

The specimens were cut in the horizontal plane along the long axis of the ganglion at a thickness of 10 μm. Every tenth section (five sections per mouse) was thaw-mounted on a MAS-coated Superfrost™ Plus microscope slide (Matsunami, Tokyo, Japan) and dried overnight at room temperature (RT; 23˚C). The five sections of each TG were used for immunohistological analysis.

After rinsing the tissue sections with 0.01 M PBS three times for 10 min each, the sections were incubated with a rabbit anti-Iba1 polyclonal antibody (1:500, 019-19741; Wako Fujifilm, Osaka, Japan) diluted in 0.01 M PBS containing 4% normal goat serum (Merck, Darmstadt, Germany) in 0.3% Triton X-100 (Merck) to identify macrophages at 4˚C for 72 h. The sections were also incubated with a rabbit polyclonal Iba1 antibody (1:500, 019-19741; Wako Fujifilm) and an Armenian hamster monoclonal CD11c antibody (1:250, ab33483; Abcam, Cambridge, UK) diluted in 0.01 M PBS containing 4% normal goat serum (Merck) in 0.3% Triton X-100 (Merck) at 4˚C for 72 h to identify Iba1-positive M1 macrophages (Iba1/CD11c).

Goat polyclonal Iba1 (1:500, ab5076; Abcam) and rabbit polyclonal mannose receptor (CD206) antibodies (1:200, ab64693; Abcam) were diluted in 0.01 M PBS containing 4% normal donkey serum (Merck) in 0.3% Triton X-100 (Merck) and incubated at 4˚C for 72 h to identify Iba1-positive M2 macrophages (Iba1/CD206).

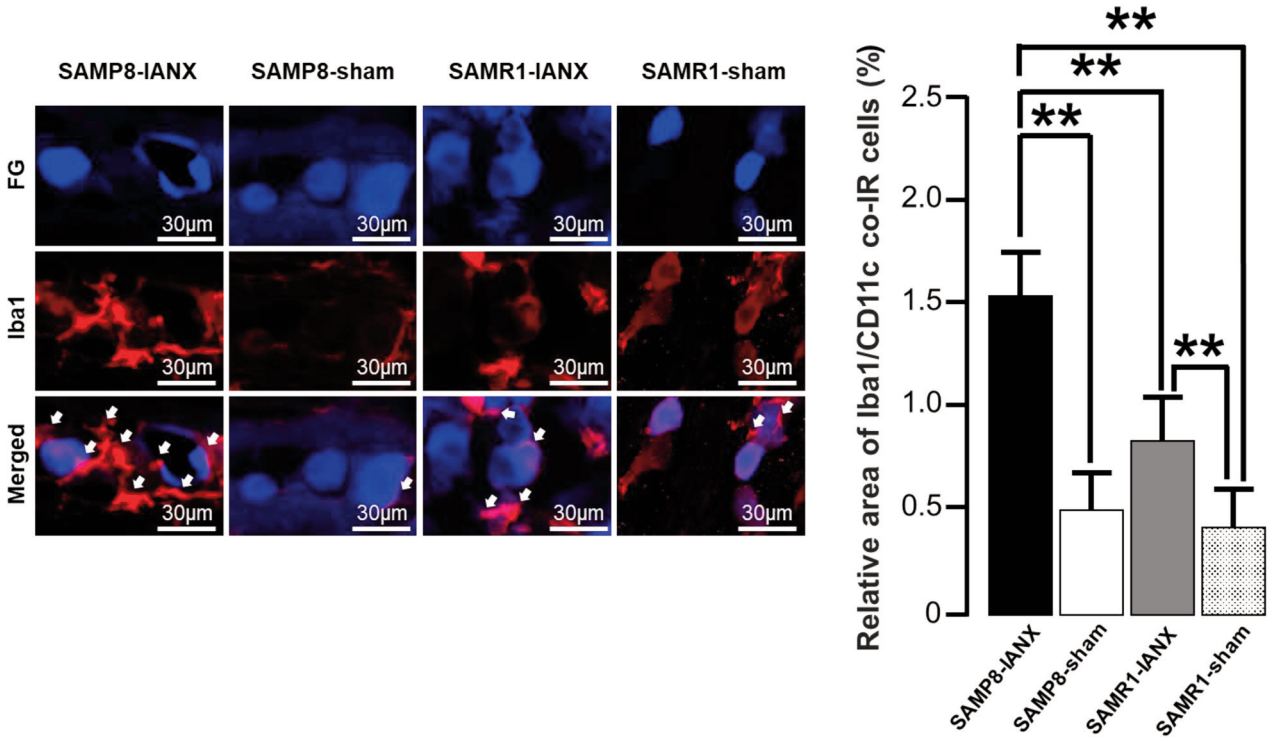

Figure 2. *Macrophages in the trigeminal ganglion (TG) on day 5 after inferior alveolar nerve transection (IANX). (A) Photomicrographs of FG-labelled Iba1-immunoreactive (IR) cells on day 5 after IANX. The arrows indicate Iba1-IR cells. Scale bars: 30 μm. (B) The relative area of Iba1-IR cells. Data represent mean±SD. (n=7 each for IANX-treated SAMP8, IANX-treated SAMR1, sham-operated SAMP8, and sham-operated SAMR1 mice; one-way ANOVA with repeated measures followed by Sidak's multiple-comparison tests, *p<0.05).*

Following primary antibody incubation, the sections were rinsed with 0.01 M PBS three times for 10 min each, and then the sections were incubated with either an Alexa Fluor® 488 donkey-anti-rabbit IgG (1:200, A-21206; Thermo Fisher Scientific, Waltham, MA, USA), Alexa Fluor® 488 goat-anti-Armenian hamster IgG (1:200, ab173003; Abcam), Alexa Fluor® 568 goat anti-rabbit IgG (1:200, ab175471; Abcam), Alexa Fluor® 568 donkey-anti-goat IgG (1:200, A-11057; Thermo fisher scientific) in 0.01 M PBS for 2 h at RT. After rinsing with 0.01 M PBS, the sections were coverslipped in PermaFluor (Thermo Fisher Scientific), and Iba1-immunoreactive (IR), Iba1/CD11c co-IR, or Iba1/CD206 co-IR cells were identified under a fluorescence microscope (BZ9000 system; Keyence, Osaka, Japan).

The areas occupied by Iba1-IR, Iba1/CD11c co-IR, or Iba1/CD206 co-IR cells found in the FG-labelled TG innervating the left whisker pad skin were analysed with an overlaid square grid (26.7×26.7 μm^2). The mean relative areas occupied by these immunostained products were measured using a computer-assisted imaging analysis system (ImageJ 1.37v; NIH, Bethesda, MD, USA). All immunohistochemical measurements were performed by observers blinded to the animal treatment status. Using the same conditions, no specific immunostaining was observed for all samples when primary antibodies were not used (negative control, data not shown).

Statistical analysis. The data are presented as mean±standard division (SD). Statistical analyses were performed using one-way or two-way repeated-measures analysis of variance (ANOVA) followed by Sidak's multiple-comparison tests, where appropriate. The cut-off for statistical significance was set at $p<0.05$. The statistical package used for the analysis by GraphPad Prism (version 5, La Jolla, CA, USA).

Results

Changes in mechanical sensitivity following IANX. The MHWT of the whisker pad skin and lower lip ipsilateral to the IANX was measured before IANX and every other day post-IANX until day 21 (Figure 1A). The MHWTs of the whisker pad skin were significantly decreased on days 1-5 in the SAMR1 mice, and days 3-11 in the SAMP8 mice ($p<0.05$). On day 5 after IANX, the MHWT values of the whisker pad skin in both SAMR1 and SAMP8 mice decreased significantly, and the MHWT of the SAMP8 mice was lower than that of SAMR1 mice (IANX-treated SAMP8 mice: 65.3±3.0 g; IANX-treated SAMR1 mice: 73.4±5.3 g; sham-operated SAMP8 mice: 82.6±1.9 g; sham-operated SAMR1 mice: 83.5±3.4 g) (Figure 1B). The MHWTs of the lower lip were significantly increased on days 1-9 in both SAMR1 mice and SAMP8 mice. On days 1-9 after IANX, there were no significant differences between MHWT in SAMP8 and SAMR1 mice (IANX-treated SAMP8

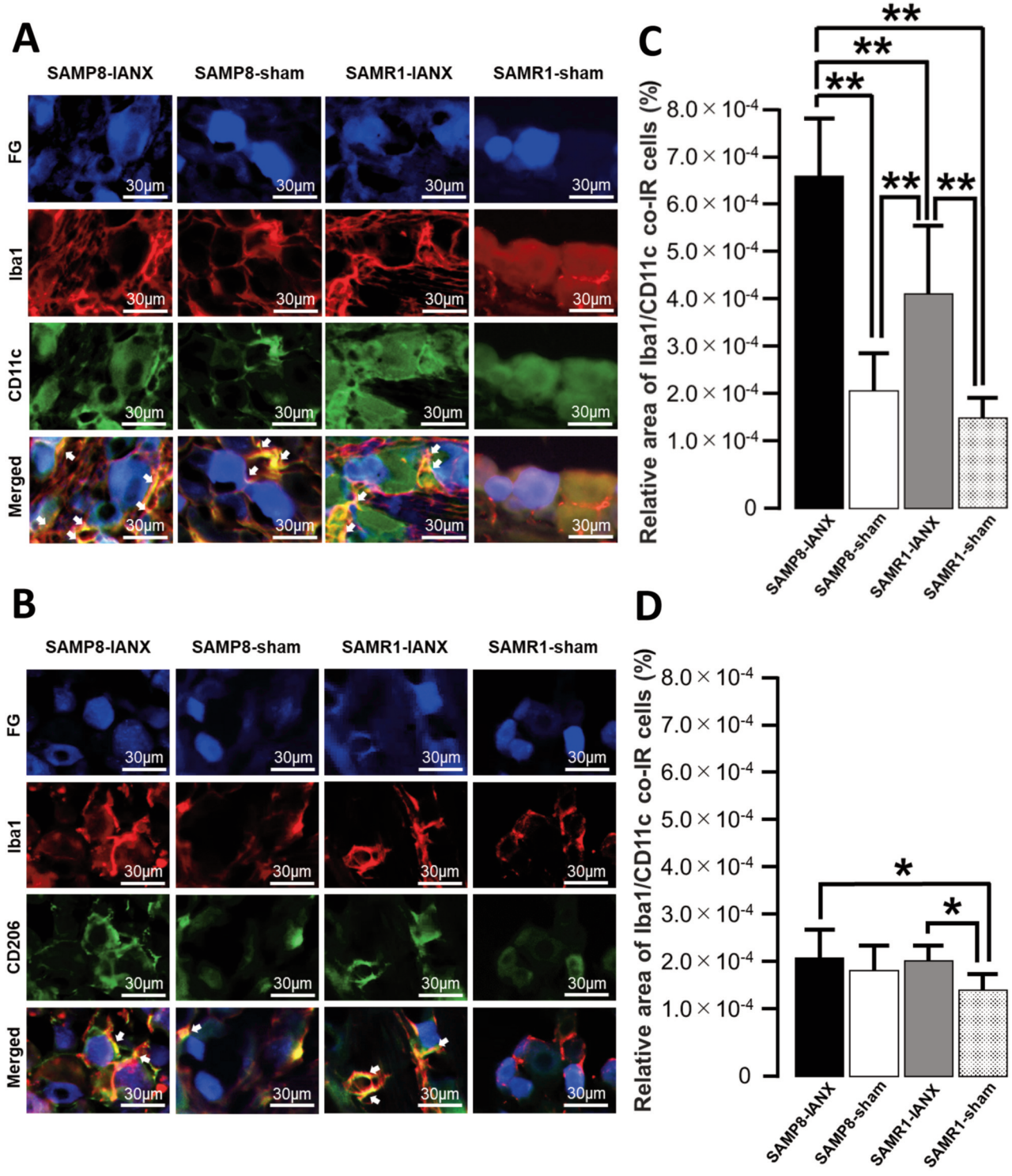

Figure 3. *M1 or M2 phenotype macrophages in TG on day 5 after inferior alveolar nerve transection (IANX). (A) Photomicrographs of Iba1/CD11c co-IR cells on day 5 after IANX. The arrows indicate Iba1/CD11c co-IR cells. Scale bars: 30 μm. (B) Photomicrographs of Iba1/CD206c co-IR cells on day 5 after IANX. The arrows indicate Iba1/CD206 co-IR cells. Scale bars: 30 μm. (C) The relative area of Iba1/CD11c co-IR cells on day 5 after IANX and sham operation. Data represent mean±SD. (n=7 each for IANX-treated SAMP8, IANX-treated SAMR1, sham-operated SAMP8, and sham-operated SAMR1 mice; one-way ANOVA with repeated measures followed by Sidak's multiple-comparison tests, **p<0.01). (D) The relative area of Iba1/CD206 co-IR cells on day 5 after IANX and sham operation. Data represent mean±SD. (n=7 each for IANX-treated SAMP8, IANX-treated SAMR1, sham-operated SAMP8, and sham-operated SAMR1 mice; one-way ANOVA with repeated measures followed by Sidak's multiple-comparison tests, *p<0.05).*

mice: 79.9±0.1 g; IANX-treated SAMR1 mice: 79.3±0.9 g; sham-operated SAMP8 mice: 64.2±0.6 g; sham-operated SAMR1 mice: 67.0±6.0 g) (Figure 1B).

Changes in Iba1, Iba1/CD11c, and Iba1/CD206 expression in TG following IANX. We examined Iba1 expression in TG on day 5 after IANX or sham operation in SAMP8 or SAMR1 mice (Figure 2A). IANX-treated SAMP8 mice exhibited significant increases in the relative area of Iba1-IR cells than sham-operated SAMP8 mice, IANX-operated SAMR1 mice, and sham-operated SAMR1 mice (IANX-treated SAMP8 mice: 1.5±0.3%; IANX-treated SAMR1 mice: 0.8±0.2%; sham-operated SAMP8 mice: 0.5±0.2%; sham-operated SAMR1 mice: 0.4±0.2%) (Figure 2B).

Next, we examined Iba1/CD11c or Iba1/CD206 expression in TG on day 5 after IANX or the sham operation in SAMP8 or SAMR1 mice (Figure 3A and B). IANX-treated SAMP8 mice exhibited significant increases in the relative area of Iba1/CD11c co-IR cells compared to those of sham-operated SAMP8, IANX-treated SAMR1, and sham-operated SAMR1 mice (IANX-treated SAMP8 mice: 6.6×10-4±1.2×10-4%; IANX-treated SAMR1 mice: $3.7\times10^{-4}\pm1.2\times10^{-4}$%; sham-operated SAMP8 mice: $2.2\times10^{-4}\pm7.3\times10^{-5}$%; sham-operated SAMR1 mice: $1.6\times10^{-4}\pm4.2\times10^{-5}$%) (Figure 3C). IANX-treated SAMP8 mice showed significant increases in the relative area of Iba1/CD206 co-IR cells compared to sham-operated SAMR1 mice. The IANX-treated SAMR1 mice exhibited significant increases in the relative area of Iba1/CD206 co-IR cells compared to sham-operated SAMR1 mice (IANX-treated SAMP8 mice: $2.1\times10^{-4}\pm5.1\times10^{-5}$%; IANX-treated SAMR1 mice: $2.1\times10^{-4}\pm2.8\times10^{-5}$%; sham-operated SAMP8 mice: $1.9\times10^{-4}\pm4.0\times10^{-5}$%; sham-operated SAMR1 mice: $1.6\times10^{-4}\pm2.8\times10^{-5}$%) (Figure 3D).

Changes in mechanical allodynia and Iba1/CD11c expression after IANX following intra-TG administration of LCCA. We examined the effect of intra-TG administration of LCCA, control-LCCA, or vehicle on mechanical pain sensitivity after IANX in SAMP8 mice on days 1-5 (Figure 4A). The administration of LCCA on IANX-treated SAMP8 mice significantly recovered the reduction in MHWT following IANX on days 3-5 compared to control-LCCA-treated, IANX-treated SAMP8 mice or vehicle-treated, IANX-treated SAMP8 mice (Figure 4B).

We investigated the effects of intra-TG administration of LCCA, control-LCCA, and vehicle on mechanical pain sensitivity of the lower lip after IANX, finding no significant differences in MHWT on days 1-5 between IANX-treated SAMP8 mice treated with LCCA, control-LCCA, or vehicle (Figure 4C).

On day 5 after IANX, we investigated the effect of LCCA, control-LCCA, or vehicle on Iba1/CD11c expression in TG in SAMP8 mice (Figure 4D). The relative areas of Iba1/CD11c co-IR cells in the IANX-treated SAMP8 mice treated with LCCA group were significantly lower compared to the control-LCCA-treated IANX-treated, SAMP8 mouse group or the vehicle-treated, IANX-treated, SAMP8 mouse group (LCCA-treated group: $1.9\times10^{-4}\pm3.9\times10^{-5}$%; control-LCCA treated group: $6.5\times10^{-4}\pm9.3\times10^{-5}$%; vehicle treated group: $6.2\times10^{-4}\pm9.7\times10^{-5}$%) (Figure 4E).

Discussion

Ectopic pain often occurs following peripheral nerve injury and inflammation. In clinical practice, older people complain of pain more frequently than young people (30). The majority of elderly people also routinely experience pain in areas with no disease or injury (31). However, the effects of ageing on ectopic pain mechanisms after peripheral nerve injury remain unclear.

Many previous studies have shown that the long-lasting mechanical allodynia observed in IANX models resembles the ectopic pain hypersensitivity observed in patients with a history of trauma to the IAN (28, 32). SAMP8 mice are an established strain that show accelerated ageing, shortened lifespans, and rapid age-dependent increases in senescence scores such as neuronal pathology; meanwhile, SAMR1 mice are a corresponding control strain of SAMP8 mice that

→

Figure 4. *Effect of intra-TG LCCA administration on mechanical sensitivity of the whisker pad skin and the number of Iba1/M1 co-IR cells after inferior alveolar nerve transection (IANX) in SAMP8 mice. (A) Time course of treatment and behavioural testing. (B) Changes in mechanical head withdrawal threshold (MHWT) of the whisker pad skin after administration with LCCA, control-LCCA, or vehicle to IANX-treated SAMP8 mice. Data represent mean±SD. (n=7 each for LCCA-administrated SAMP8, control-LCCA-administrated SAMP8, vehicle-administrated SAMP8 mice; two-way repeated-measures analysis of variance followed by Sidak's multiple-comparison tests, **p<0.01, LCCA-administrated SAMP8 vs. control-LCCA-administrated SAMP8 mice. ++p<0.01, LCCA-administrated SAMP8 vs. vehicle-administrated SAMP8 mice). (C) Changes in MHWT of the lower lip after administration with LCCA or control-LCCA or vehicle to IANX-treated SAMP8 mice. Data represent mean±SD. (n=7 each for LCCA-administrated SAMP8, control-LCCA-administrated SAMP8, vehicle-administrated SAMP8 mice; two-way repeated-measures analysis of variance followed by Sidak's multiple-comparison tests, **p<0.01, LCCA-administrated SAMP8 vs. control-LCCA-administrated SAMP8 mice. ++p<0.01, LCCA-administrated SAMP8 vs. vehicle-administrated SAMP8 mice). (D) Photomicrographs of Iba1/CD11c co-IR cells on day 5 after IANX. The arrows indicate Iba1/CD11c co-IR cells. Scale bars: 30 μm. (E) The relative area of Iba1/CD11c co-IR cells on day 5 after IANX and sham operation. Data represent mean±SD. (n=7 each for LCCA-administrated SAMP8, control-LCCA-administrated SAMP8, and vehicle-administrated SAMP8 mice; one-way ANOVA with repeated measures followed by Sidak's multiple-comparison tests, **p<0.01).*

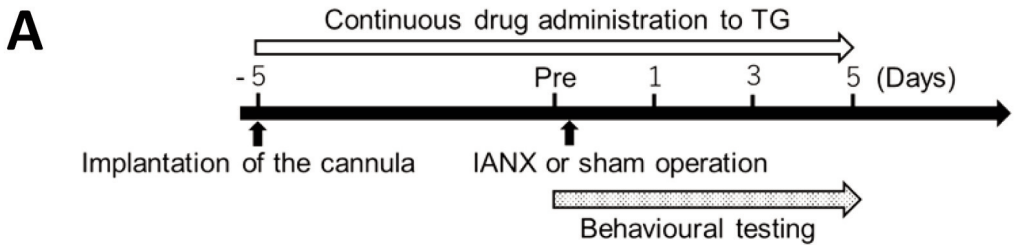
A
Continuous drug administration to TG
-5
Pre
1
3
5 (Days)
Implantation of the cannula
IANX or sham operation
Behavioural testing

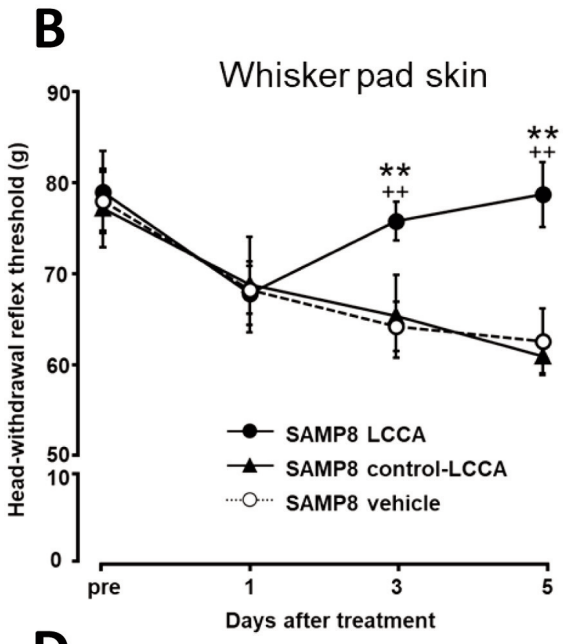
B
Whisker pad skin
Head-withdrawal reflex threshold (g)
90
80
70
60
50
10
0
**
++
SAMP8 LCCA
SAMP8 control-LCCA
SAMP8 vehicle
pre
1
3
5
Days after treatment

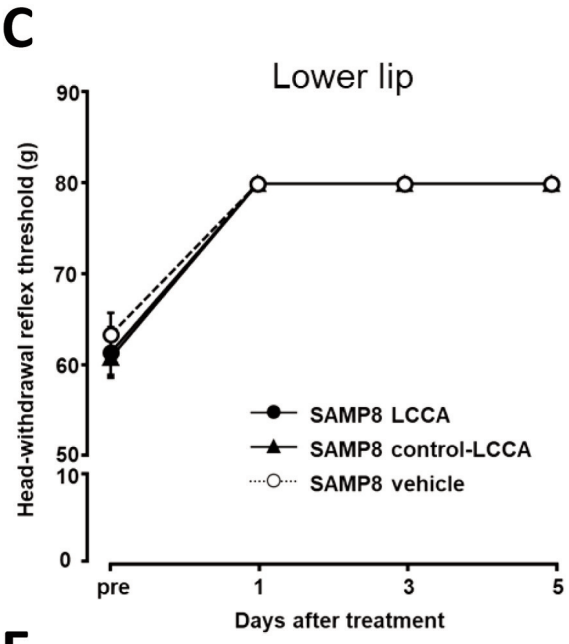
C
Lower lip
Head-withdrawal reflex threshold (g)
90
80
70
60
50
10
0
SAMP8 LCCA
SAMP8 control-LCCA
SAMP8 vehicle
pre
1
3
5
Days after treatment

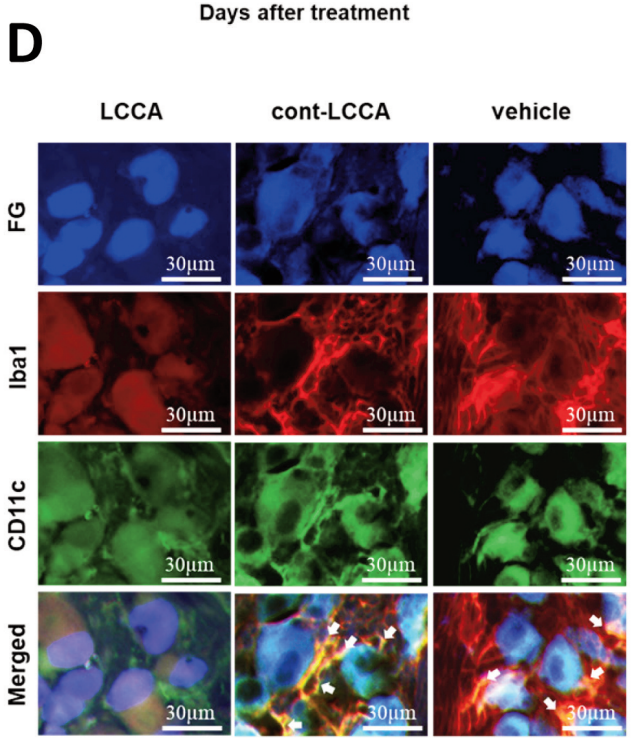
D
LCCA
cont-LCCA
vehicle
FG
Iba1
CD11c
Merged
30μm

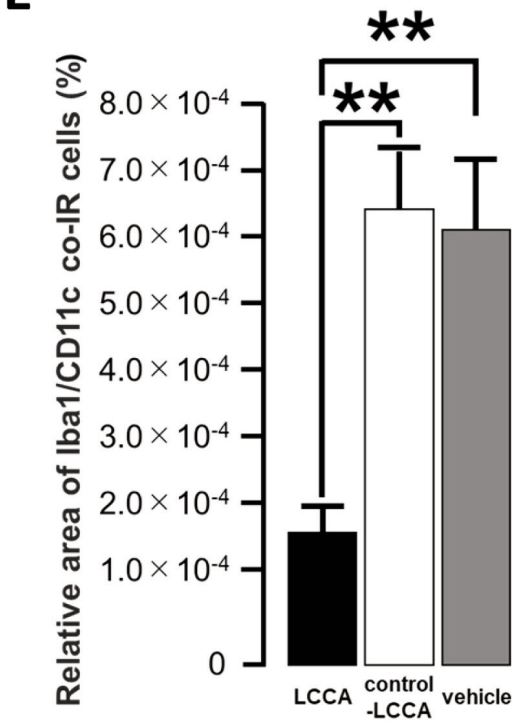
E
**
**
Relative area of Iba1/CD11c co-IR cells (%)
8.0 × 10-4
7.0 × 10-4
6.0 × 10-4
5.0 × 10-4
4.0 × 10-4
3.0 × 10-4
2.0 × 10-4
1.0 × 10-4
0
LCCA
control -LCCA
vehicle

exhibit normal ageing (24, 33, 34). Compared to several other SAMP strain mice, SAMP8 mice exhibit physiological and morphological features that better resemble ageing-related changes found in human brains (35). Thus, examining neuropathological differences between SAMP8 and SAMR1 mice at the same time point should be appropriate for determining the effects of ageing on neural mechanisms (21, 24, 36).

Here, both SAMP8 and SAMR1 mice developed mechanical allodynia of the whisker pad skin after IANX. Interestingly, SAMP8 mice developed stronger mechanical allodynia than that of SAMR1 mice post-IANX. In addition, both SAMP8 and SAMR1 mice showed increased MHWT in the lower lip post-IANX. This result is similar to that produced by lower lip dysesthesia in humans following alveolar nerve injury. Therefore, using IANX-treated SAMP8 mouse may be useful for studying the effects of ageing on the mechanism of orofacial ectopic pain.

Many previous studies have indicated that peripheral nerve injury increases the number of resident and proliferated macrophages in sensory ganglia (37-39). Iba1 expression is a specific marker for macrophages (40). Here, the number of Iba1-IR cells in the TG increased on day 5 after IANX and mechanical allodynia of the whisker pad skin was enhanced in SAMP8 mice. Furthermore, Iba1-IR cells were more abundant in the TG of SAMP8 mice than in SAMR1 mice on day 5 after IANX. Previous studies have shown that IANX increased the number of Iba1-IR cells in TG and induced mechanical allodynia in the whisker pad skin (29). An animal model of persistent peripheral neuropathic pain, the spared nerve injury model, develops mechanical allodynia in the plantar surface of the hind paw (41). In this rat model, ageing enhances the increased expression of Iba-1 IR cells in nociceptive neurons compared to young rats (42). These reports agree with our present results, suggesting that ageing enhances the increase in Iba1-IR cell expression in the TG at the onset of ectopic mechanical allodynia in whisker pad skin after IANX. M1 macrophages potentiate inflammation by producing TNF-α, interleukins (IL)-6, and C-C motif chemokine 2 (CCL2) (43-45). In contrast, M2 macrophages function as anti-inflammatory agents by producing anti-inflammatory products such as IL-4, transforming growth factor-β, and CCL4 (46-48). Some previous reports have also indicated that CD11c is a major marker for M1 macrophages (49, 50), and that CD206 is a major marker for M2 macrophage activation states (50, 51).

We examined Iba1/CD11c co-IR cells, or Iba1/CD206 co-IR cells in the TG on day 5 after IANX and found that Iba1/CD11c co-IR cells were increased in both SAMP8 and SAMR1 mice. Moreover, the number of Iba1/CD11c co-IR cells in SAMP8 mice was greater than that of SAMR1 mice. Meanwhile, Iba1/CD206 co-IR cells were increased in SAMR1 mice following IANX, but no significant differences were observed in corresponding SAMP8 mice.

Macrophage polarity changes are related to ageing. Ageing has widely been reported to accelerate the polarity switch from M2-like to M1-like macrophages (52-54). Further, macrophages in the enteric nervous system reportedly exhibit enhanced inflammatory M1 polarity following ageing, resulting in enhanced neural responses to inflammatory signals (55). Consistent with these reports, our present results suggest that age-related macrophage polarity changes in TG accelerate changes in inflammatory M1 polarity, which enhances mechanical allodynia in whisker pad skin after IANX. Additionally, many other markers for M1 have been found, such as CD38, CD86, and CD40 (56, 57). Future studies using other M1 and M2 markers may be necessary to investigate the involvement of macrophage polarity changes in orofacial ectopic pain.

When LCCA, a macrophage depleting agent, was directly and continuously administered into the TG in SAMP8 mice, mechanical allodynia of whisker pad skin on day 5 after IANX was significantly suppressed compared to the control-LCCA-treated and vehicle-treated SAMP8 mice. We confirmed that the increase in the number of Iba1/CD11c co-IR cells in TG on day 5 after IANX was significantly suppressed in LCCA-treated SAMP8 mice compared to the control-LCCA or vehicle-treated SAMP8 mice. Previous studies have reported that IANX enhances background activity and responsiveness to mechanical stimuli in the infraorbital nerve (28, 58), resulting in the development of ectopic mechanical allodynia in the ipsilateral whisker pad skin (59). The various macrophage-derived pro-nociceptive mediators induce neuronal sensitization and hyperexcitation (60). Increased ageing-related neural responses to inflammatory signals involve a shift in macrophage polarity from an anti-inflammatory M2 to an inflammatory M1 state (55). In the spinal cord, TNF-α released from M1 macrophages binds to TNF receptor-α1 on nociceptive neurons, causing neuronal sensitization, and leading to cutaneous mechanical allodynia (60). Furthermore, other reports indicate that TNF-α released from accumulated M1 macrophages activates satellite cells following the injury of dorsal root ganglion neurons innervating the colon; neural hyperexcitation of the injured primary sensory neuron of the colon enhanced the excitability of primary sensory neuron innervating the uninjured bladder, causing bladder dysfunction and hypersensitivity (61, 62). Furthermore, orofacial ectopic pain studies have indicated that neuron-macrophage interactions are involved in the pathogenesis of abnormal tongue pain after pulpitis by enhancing TG neuronal excitability *via* IL-1 receptor type-1 and transient receptor potential vanilloid-1 signalling (63). Together, these reports indicate that macrophages in TG directly or indirectly enhanced the excitability of neurons, innervating areas remote from the injured area, which play a

key role in the development of orofacial ectopic pain. Our results agree with these past reports, also indicating that age-related changes in macrophage expression in TG are responsible for worsening mechanical allodynia of the whisker pad skin, and that these changes enhance the excitability of TG neurons after IANX. However, to further corroborate this, macrophage-mediated changes in TG neuronal excitability after IANX need to be clarified in SAMP8 mice.

In conclusion, the ectopic mechanical allodynia that develops in the whisker pad skin after IANX is enhanced with ageing, and the enhanced age-related inflammatory M1 macrophage polarity changes seen in the TG play a pivotal role in this pathogenesis. This present study is the first report regarding the effects of ageing on orofacial ectopic pain. The results of this study should facilitate the elucidation of the regulatory mechanisms of abnormal pain associated with ageing.

Conflicts of Interest

The Authors declare that there are no conflicts of interest in relation to this study.

Authors' Contributions

Conceptualization: S.F., K.U., T.I., K.I., and M.S.; methodology: S.F., T.O., K.U., and M.S.; validation: T.O., Y.H., S.H., T.I., and K.I.; formal analysis: S.F., Y.H., S.H., K.U, and M.S; investigation: S.F., T.O., and K.U; data curation: S.F.; writing – original draft preparation; S.F., K.U; writing – review and editing: K.U., and M.S; visualization: S.F.; supervision: K.U. and M.S; project administration: K.U. funding acquisition: K.U., and M.S. All Authors have read and agreed to the published version of the manuscript.

Acknowledgements

This study was supported in part by grants from the Sato Fund, Uemura Fund, and Dental Research Center at Nihon University School of Dentistry, Tokyo, Japan, KAKENHI (22K10064, 20K18619). The Authors would like to thank all the members of the Department of Complete Denture Prosthodontics and the Department of Physiology of Nihon University School of Dentistry. The Authors also thank Editage (www.editage.jp) for the English language editing.

References

1 Khawaja N and Renton T: Case studies on implant removal influencing the resolution of inferior alveolar nerve injury. Br Dent J *206(7)*: 365-370, 2009. PMID: 19357667. DOI: 10.1038/sj.bdj.2009.258

2 Meyer RA and Bagheri SC: Long-term outcome of trigeminal nerve injuries related to dental treatment. J Oral Maxillofac Surg *69(12)*: 2946, 2011. PMID: 22117703. DOI: 10.1016/j.joms.2011.09.018

3 Yang J, Liu F, Zhang YY, Lin J, Li YL, Zhou C, Li CJ and Shen JF: C-X-C motif chemokine ligand 1 and its receptor C-X-C motif chemokine receptor 2 in trigeminal ganglion contribute to nerve injury-induced orofacial mechanical allodynia. J Oral Rehabil *49(2)*: 195-206, 2022. PMID: 34714950. DOI: 10.1111/joor.13273

4 Huang CL, Liu F, Zhang YY, Lin J, Fu M, Li YL, Zhou C, Li CJ and Shen JF: Activation of oxytocin receptor in the trigeminal ganglion attenuates orofacial ectopic pain attributed to inferior alveolar nerve injury. J Neurophysiol *125(1)*: 223-231, 2021. PMID: 33326336. DOI: 10.1152/jn.00646.2020

5 Bai L, Wang X, Li Z, Kong C, Zhao Y, Qian JL, Kan Q, Zhang W and Xu JT: Upregulation of chemokine CXCL12 in the dorsal root ganglia and spinal cord contributes to the development and maintenance of neuropathic pain following spared nerve injury in rats. Neurosci Bull *32(1)*: 27-40, 2016. PMID: 26781879. DOI: 10.1007/s12264-015-0007-4

6 Ji RR, Chamessian A and Zhang YQ: Pain regulation by non-neuronal cells and inflammation. Science *354(6312)*: 572-577, 2016. PMID: 27811267. DOI: 10.1126/science.aaf8924

7 Gold MS, Weinreich D, Kim CS, Wang R, Treanor J, Porreca F and Lai J: Redistribution of Na(V)1.8 in uninjured axons enables neuropathic pain. J Neurosci *23(1)*: 158-166, 2003. PMID:12514212.

8 Komiya H, Shimizu K, Noma N, Tsuboi Y, Honda K, Kanno K, Ohara K, Shinoda M, Ogiso B and Iwata K: Role of neuron-glial interaction mediated by IL-1β in ectopic tooth pain. J Dent Res *97(4)*: 467-475, 2018. PMID: 29131694. DOI: 10.1177/0022034517741253

9 Cherkas PS, Huang TY, Pannicke T, Tal M, Reichenbach A and Hanani M: The effects of axotomy on neurons and satellite glial cells in mouse trigeminal ganglion. Pain *110(1-2)*: 290-298, 2004. PMID: 15275779. DOI: 10.1016/j.pain.2004.04.007

10 Iwata K and Shinoda M: Role of neuron and non-neuronal cell communication in persistent orofacial pain. J Dent Anesth Pain Med *19(2)*: 77-82, 2019. PMID: 31065589. DOI: 10.17245/jdapm.2019.19.2.77

11 Shinoda M, Kubo A, Hayashi Y and Iwata K: Peripheral and central mechanisms of persistent orofacial pain. Front Neurosci *13*: 1227, 2019. PMID: 31798407. DOI: 10.3389/fnins.2019.01227

12 Iwata K, Katagiri A and Shinoda M: Neuron-glia interaction is a key mechanism underlying persistent orofacial pain. J Oral Sci *59(2)*: 173-175, 2017. PMID: 28637974. DOI: 10.2334/josnusd.16-0858

13 Sprangers S, de Vries TJ and Everts V: Monocyte heterogeneity: Consequences for monocyte-derived immune cells. J Immunol Res *2016*: 1475435, 2016. PMID: 27478854. DOI: 10.1155/2016/1475435

14 Brown BN, Ratner BD, Goodman SB, Amar S and Badylak SF: Macrophage polarization: an opportunity for improved outcomes in biomaterials and regenerative medicine. Biomaterials *33(15)*: 3792-3802, 2012. PMID: 22386919. DOI: 10.1016/j.biomaterials.2012.02.034

15 Franco R and Fernández-Suárez D: Alternatively activated microglia and macrophages in the central nervous system. Prog Neurobiol *131*: 65-86, 2015. PMID: 26067058. DOI: 10.1016/j.pneurobio.2015.05.003

16 Nadeau S, Filali M, Zhang J, Kerr BJ, Rivest S, Soulet D, Iwakura Y, de Rivero Vaccari JP, Keane RW and Lacroix S: Functional recovery after peripheral nerve injury is dependent on the pro-inflammatory cytokines IL-1β and TNF: implications for neuropathic pain. J Neurosci *31(35)*: 12533-12542, 2011. PMID: 21880915. DOI: 10.1523/JNEUROSCI.2840-11.2011

17 Sica A and Mantovani A: Macrophage plasticity and polarization: in vivo veritas. J Clin Invest *122(3)*: 787-795, 2012. PMID: 22378047. DOI: 10.1172/JCI59643

18 Davis MP and Srivastava M: Demographics, assessment and management of pain in the elderly. Drugs Aging *20(1)*: 23-57, 2003. PMID: 12513114. DOI: 10.2165/00002512-200320010-00003

19 Ma W, Chabot JG, Vercauteren F and Quirion R: Injured nerve-derived COX2/PGE2 contributes to the maintenance of neuropathic pain in aged rats. Neurobiol Aging *31(7)*: 1227-1237, 2010. PMID: 18786748. DOI: 10.1016/j.neurobiolaging.2008.08.002

20 Galbavy W, Kaczocha M, Puopolo M, Liu L and Rebecchi MJ: Neuroimmune and neuropathic responses of spinal cord and dorsal root ganglia in middle age. PLoS One *10(8)*: e0134394, 2015. PMID: 26241743. DOI: 10.1371/journal.pone.0134394

21 Ikutame D, Urata K, Oto T, Fujiwara S, Iinuma T, Shibuta I, Hayashi Y, Hitomi S, Iwata K and Shinoda M: Aging-related phenotypic conversion of medullary microglia enhances intraoral incisional pain sensitivity. Int J Mol Sci *21(21)*: 7871, 2020. PMID: 33114176. DOI: 10.3390/ijms21217871

22 Liu B, Liu J and Shi JS: SAMP8 mice as a model of age-related cognition decline with underlying mechanisms in Alzheimer's disease. J Alzheimers Dis *75(2)*: 385-395, 2020. PMID: 32310176. DOI: 10.3233/JAD-200063

23 Takeda T: Senescence-accelerated mouse (SAM) with special references to neurodegeneration models, SAMP8 and SAMP10 mice. Neurochem Res *34(4)*: 639-659, 2009. PMID: 19199030. DOI: 10.1007/s11064-009-9922-y

24 Takeda T, Hosokawa M, Higuchi K, Hosono M, Akiguchi I and Katoh H: A novel murine model of aging, senescence-accelerated mouse (SAM). Arch Gerontol Geriatr *19(2)*: 185-192, 1994. PMID: 15374284. DOI: 10.1016/0167-4943(94)90039-6

25 Takeda T, Hosokawa M and Higuchi K: Senescence-accelerated mouse (SAM): a novel murine model of senescence. Exp Gerontol *32(1-2)*: 105-109, 1997. PMID: 9088907. DOI: 10.1016/s0531-5565(96)00036-8

26 Miyamoto M, Kiyota Y, Yamazaki N, Nagaoka A, Matsuo T, Nagawa Y and Takeda T: Age-related changes in learning and memory in the senescence-accelerated mouse (SAM). Physiol Behav *38(3)*: 399-406, 1986. PMID: 3786521. DOI: 10.1016/0031-9384(86)90112-5

27 Zimmermann M: Ethical guidelines for investigations of experimental pain in conscious animals. Pain *16(2)*: 109-110, 1983. PMID: 6877845. DOI: 10.1016/0304-3959(83)90201-4

28 Iwata K, Imai T, Tsuboi Y, Tashiro A, Ogawa A, Morimoto T, Masuda Y, Tachibana Y and Hu J: Alteration of medullary dorsal horn neuronal activity following inferior alveolar nerve transection in rats. J Neurophysiol *86(6)*: 2868-2877, 2001. PMID: 11731543. DOI: 10.1152/jn.2001.86.6.2868

29 Batbold D, Shinoda M, Honda K, Furukawa A, Koizumi M, Akasaka R, Yamaguchi S and Iwata K: Macrophages in trigeminal ganglion contribute to ectopic mechanical hypersensitivity following inferior alveolar nerve injury in rats. J Neuroinflammation *14(1)*: 249, 2017. PMID: 29246259. DOI: 10.1186/s12974-017-1022-3

30 Dubský M, Fejfarova V, Bem R and Jude EB: Pain management in older adults with chronic wounds. Drugs Aging *39(8)*: 619-629, 2022. PMID: 35829959. DOI: 10.1007/s40266-022-00963-w

31 Hanks-Bell M, Halvey K and Paice JA: Pain assessment and management in aging. Online J Issues Nurs *9(3)*: 8, 2004. PMID: 15482094.

32 Kaji K, Shinoda M, Honda K, Unno S, Shimizu N and Iwata K: Connexin 43 contributes to ectopic orofacial pain following inferior alveolar nerve injury. Mol Pain *12*: 1744806916633704, 2016. PMID: 27030716. DOI: 10.1177/1744806916633704

33 Takeda T, Hosokawa M and Higuchi K: Senescence-accelerated mouse (SAM): a novel murine model of accelerated senescence. J Am Geriatr Soc *39(9)*: 911-919, 1991. PMID: 1885867. DOI: 10.1111/j.1532-5415.1991.tb04460.x

34 Butterfield DA and Poon HF: The senescence-accelerated prone mouse (SAMP8): a model of age-related cognitive decline with relevance to alterations of the gene expression and protein abnormalities in Alzheimer's disease. Exp Gerontol *40(10)*: 774-783, 2005. PMID: 16026957. DOI: 10.1016/j.exger.2005.05.007

35 Akiguchi I, Pallàs M, Budka H, Akiyama H, Ueno M, Han J, Yagi H, Nishikawa T, Chiba Y, Sugiyama H, Takahashi R, Unno K, Higuchi K and Hosokawa M: SAMP8 mice as a neuropathological model of accelerated brain aging and dementia: Toshio Takeda's legacy and future directions. Neuropathology *37(4)*: 293-305, 2017. PMID: 28261874. DOI: 10.1111/neup.12373

36 Kong D, Yan Y, He XY, Yang H, Liang B, Wang J, He Y, Ding Y and Yu H: Effects of resveratrol on the mechanisms of antioxidants and estrogen in Alzheimer's disease. Biomed Res Int 2019: 8983752, 2019. PMID: 31016201. DOI: 10.1155/2019/8983752

37 Yu X, Liu H, Hamel KA, Morvan MG, Yu S, Leff J, Guan Z, Braz JM and Basbaum AI: Dorsal root ganglion macrophages contribute to both the initiation and persistence of neuropathic pain. Nat Commun *11(1)*: 264, 2020. PMID: 31937758. DOI: 10.1038/s41467-019-13839-2

38 Kwon MJ, Kim J, Shin H, Jeong SR, Kang YM, Choi JY, Hwang DH and Kim BG: Contribution of macrophages to enhanced regenerative capacity of dorsal root ganglia sensory neurons by conditioning injury. J Neurosci *33(38)*: 15095-15108, 2013. PMID: 24048840. DOI: 10.1523/JNEUROSCI.0278-13.2013

39 Kim D, You B, Lim H and Lee SJ: Toll-like receptor 2 contributes to chemokine gene expression and macrophage infiltration in the dorsal root ganglia after peripheral nerve injury. Mol Pain *7*: 74, 2011. PMID: 21951975. DOI: 10.1186/1744-8069-7-74

40 Ohsawa K, Imai Y, Sasaki Y and Kohsaka S: Microglia/macrophage-specific protein Iba1 binds to fimbrin and enhances its actin-bundling activity. J Neurochem *88(4)*: 844-856, 2004. PMID: 14756805. DOI: 10.1046/j.1471-4159.2003.02213.x

41 Decosterd I and Woolf CJ: Spared nerve injury: an animal model of persistent peripheral neuropathic pain. Pain *87(2)*: 149-158, 2000. PMID: 10924808. DOI: 10.1016/S0304-3959(00)00276-1

42 Vega-Avelaira D, Moss A and Fitzgerald M: Age-related changes in the spinal cord microglial and astrocytic response profile to nerve injury. Brain Behav Immun *21(5)*: 617-623, 2007. PMID: 17158026. DOI: 10.1016/j.bbi.2006.10.007

43 Zheng Q, Zhang J, Zuo X, Sun J, Liang Z, Hu X, Wang Z, Li K, Song J, Ding T, Shen X, Ma Y and Li P: Photobiomodulation promotes neuronal axon regeneration after oxidative stress and induces a change in polarization from M1 to M2 in macrophages *via* stimulation of CCL2 in neurons: relevance to spinal cord injury. J Mol Neurosci *71(6)*: 1290-1300, 2021. PMID: 33417168. DOI: 10.1007/s12031-020-01756-9

44 Benoit M, Desnues B and Mege JL: Macrophage polarization in bacterial infections. J Immunol *181(6)*: 3733-3739, 2008. PMID: 18768823. DOI: 10.4049/jimmunol.181.6.3733

45 Chen O, Donnelly CR and Ji RR: Regulation of pain by neuro-immune interactions between macrophages and nociceptor sensory neurons. Curr Opin Neurobiol *62*: 17-25, 2020. PMID: 31809997. DOI: 10.1016/j.conb.2019.11.006
46 Mantovani A, Sozzani S, Locati M, Allavena P and Sica A: Macrophage polarization: tumor-associated macrophages as a paradigm for polarized M2 mononuclear phagocytes. Trends Immunol *23(11)*: 549-555, 2002. PMID: 12401408. DOI: 10.1016/s1471-4906(02)02302-5
47 Wu BM, Liu JD, Li YH and Li J: Margatoxin mitigates CCl4 induced hepatic fibrosis in mice *via* macrophage polarization, cytokine secretion and STAT signaling. Int J Mol Med *45(1)*: 103-114, 2020. PMID: 31746414. DOI: 10.3892/ijmm.2019.4395
48 Gordon S: Alternative activation of macrophages. Nat Rev Immunol *3(1)*: 23-35, 2003. PMID: 12511873. DOI: 10.1038/nri978
49 Lumeng CN, DelProposto JB, Westcott DJ and Saltiel AR: Phenotypic switching of adipose tissue macrophages with obesity is generated by spatiotemporal differences in macrophage subtypes. Diabetes *57(12)*: 3239-3246, 2008. PMID: 18829989. DOI: 10.2337/db08-0872
50 Kigerl KA, Gensel JC, Ankeny DP, Alexander JK, Donnelly DJ and Popovich PG: Identification of two distinct macrophage subsets with divergent effects causing either neurotoxicity or regeneration in the injured mouse spinal cord. J Neurosci *29(43)*: 13435-13444, 2009. PMID: 19864556. DOI: 10.1523/JNEUROSCI.3257-09.2009
51 Viola A, Munari F, Sánchez-Rodríguez R, Scolaro T and Castegna A: The metabolic signature of macrophage responses. Front Immunol *10*: 1462, 2019. PMID: 31333642. DOI: 10.3389/fimmu.2019.01462
52 Kang K, Park SH, Chen J, Qiao Y, Giannopoulou E, Berg K, Hanidu A, Li J, Nabozny G, Kang K, Park-Min KH and Ivashkiv LB: Interferon-γ represses M2 gene expression in human macrophages by disassembling enhancers bound by the transcription factor MAF. Immunity *47(2)*: 235-250.e4, 2017. PMID: 28813657. DOI: 10.1016/j.immuni.2017.07.017
53 Yamaguchi Y, Kaida K, Suenaga Y, Ishigami A, Kobayashi Y and Nagata K: Age-related dysfunction of p53-regulated phagocytic activity in macrophages. Biochem Biophys Res Commun *529(2)*: 462-466, 2020. PMID: 32703452. DOI: 10.1016/j.bbrc.2020.05.121
54 Takahashi R, Ishigami A, Kobayashi Y and Nagata K: Skewing of peritoneal resident macrophages toward M1-like is involved in enhancement of inflammatory responses induced by secondary necrotic neutrophils in aged mice. Cell Immunol *304-305*: 44-48, 2016. PMID: 26965995. DOI: 10.1016/j.cellimm.2016.03.001
55 Becker L, Nguyen L, Gill J, Kulkarni S, Pasricha PJ and Habtezion A: Age-dependent shift in macrophage polarisation causes inflammation-mediated degeneration of enteric nervous system. Gut *67(5)*: 827-836, 2018. PMID: 28228489. DOI: 10.1136/gutjnl-2016-312940
56 Amici SA, Young NA, Narvaez-Miranda J, Jablonski KA, Arcos J, Rosas L, Papenfuss TL, Torrelles JB, Jarjour WN and Guerau-de-Arellano M: CD38 is robustly induced in human macrophages and monocytes in inflammatory conditions. Front Immunol *9*: 1593, 2018. PMID: 30042766. DOI: 10.3389/fimmu.2018.01593
57 Ley K, Gerdes N and Winkels H: ATVB distinguished scientist award: How costimulatory and coinhibitory pathways shape atherosclerosis. Arterioscler Thromb Vasc Biol *37(5)*: 764-777, 2017. PMID: 28360089. DOI: 10.1161/ATVBAHA.117.308611
58 Tsuboi Y, Takeda M, Tanimoto T, Ikeda M, Matsumoto S, Kitagawa J, Teramoto K, Simizu K, Yamazaki Y, Shima A, Ren K and Iwata K: Alteration of the second branch of the trigeminal nerve activity following inferior alveolar nerve transection in rats. Pain *111(3)*: 323-334, 2004. PMID: 15363876. DOI: 10.1016/j.pain.2004.07.014
59 Nomura H, Ogawa A, Tashiro A, Morimoto T, Hu JW and Iwata K: Induction of Fos protein-like immunoreactivity in the trigeminal spinal nucleus caudalis and upper cervical cord following noxious and non-noxious mechanical stimulation of the whisker pad of the rat with an inferior alveolar nerve transection. Pain *95(3)*: 225-238, 2002. PMID: 11839422. DOI: 10.1016/S0304-3959(01)00403-1
60 Domoto R, Sekiguchi F, Tsubota M and Kawabata A: Macrophage as a peripheral pain regulator. Cells *10(8)*: 1881, 2021. PMID: 34440650. DOI: 10.3390/cells10081881
61 Qiao LY and Tiwari N: Spinal neuron-glia-immune interaction in cross-organ sensitization. Am J Physiol Gastrointest Liver Physiol *319(6)*: G748-G760, 2020. PMID: 33084399. DOI: 10.1152/ajpgi.00323.2020
62 Panicker JN, Marcelissen T, von Gontard A, Vrijens D, Abrams P and Wyndaele M: Bladder-bowel interactions: Do we understand pelvic organ cross-sensitization? International Consultation on Incontinence Research Society (ICI-RS) 2018. Neurourol Urodyn *38(Suppl 5)*: S25-S34, 2019. PMID: 31821639. DOI: 10.1002/nau.24111
63 Kanno K, Shimizu K, Shinoda M, Hayashi M, Takeichi O and Iwata K: Role of macrophage-mediated Toll-like receptor 4-interleukin-1R signaling in ectopic tongue pain associated with tooth pulp inflammation. J Neuroinflammation *17(1)*: 312, 2020. PMID: 33081813. DOI: 10.1186/s12974-020-01995-y

Received October 27, 2022
Revised November 5, 2022
Accepted November 7, 2022